



Characterization of coacervation behavior between whey protein isolate and gum Arabic: Effects of heat treatment

Xiaoshan Wan^{a,1}, Meihui Zhao^{a,1}, Mengxue Guo^a, Peng Li^a, Haohao Shi^a, Xueying Zhang^a, Zhongyuan Liu^a, Guanghua Xia^{a,b,*}

^a Hainan Engineering Research Center of Aquatic Resources Efficient Utilization in South China Sea, Key Laboratory of Food Nutrition and Functional Food of Hainan Province, Key Laboratory of Seafood Processing of Haikou, Engineering Research Center of Utilization of Tropical Polysaccharide Resources of MOE, College of Food Science and Technology, Hainan University, Hainan 570228, China

^b Collaborative Innovation Center of Provincial and Ministerial Co-Construction for Marine Food Deep Processing, Dalian Polytechnic University, Dalian 116034, China

ARTICLE INFO

Keywords:

Coacervation
Whey protein isolate
Arabic gum
Non-covalent complex

ABSTRACT

Currently, the effect of heat treatment on the complex coacervation behavior of whey isolate protein (WPI) with gum arabic (GA) is undiscussed. In this work, the complex coacervation behavior of WPI with or without heat treatment and GA in different environments was investigated. The results showed that coacervates were formed at a mass ratio of 2:1 and a pH of 3.5, which was confirmed by the fluorescence spectroscopy results. Heat treatment increased the surface charge of WPI, reduced the saturated adsorption concentration of GA, and enhanced the sensitivity of the complex coacervation reaction to salt ions. Fourier infrared spectroscopy, intermolecular force analysis and molecular docking results confirm that the formation of coacervates is the result of electrostatic interactions. From the scanning electron microscope and differential scanning calorimetry results, it is clear that the whey isolate protein combined with gum arabic forms a gel-like conjugate with higher thermal stability and a dense structure. This study provides more in-depth theoretical guidance for the application of WPI and GA based coacervation and more advanced theoretical data for the study of hWPI.

1. Introduction

A complex coacervation reaction is when two or more oppositely charged polymeric electrolytes contained in a solution system combine by multiple forces to generate coacervate (Cabezas et al., 2019). Complex coacervation reactions are an attractive method for the preparation of complexes (Wang et al., 2022). Compared to single substances, complex coacervates tend to have a more dense structure (Zou, et al., 2020) and exhibit superior thermal stability (Tavares et al., 2021; Zhang et al., 2020) and resistance to mechanical shear (Xiong et al., 2016). This makes the coacervates have numerous advantages, including controlled release, biocompatibility, easy of decomposition, and easy of loading, as well as the potential for application in different food applications like functional substance delivery carriers (Muhoza et al., 2022; Zhang et al., 2021), edible films (Tavares et al., 2021), fat substitution (Huang et al., 2022), protein extraction and purification (Yang et al., 2020). Therefore,

a better understanding of complex coacervation reactions is necessary for further applications.

In food industries, protein and anionic polysaccharides are the main raw materials for the preparation of complex coacervate (Muhoza et al., 2022). The formation of complex coacervate is mainly influenced by two types of factors: raw material properties (type of charged groups, position of charged groups, charge, etc.) (Comunian et al., 2022; Pillai et al., 2019) and environmental conditions (salt ion type, salt ion strength, pH, protein/polysaccharide ratio, total polymer concentration, temperature, etc.) (Liu et al., 2015; Niu et al., 2015). Thus, the behavior of complex coacervation changes when the environmental conditions of the solution system are changed. During the shift of solution pH from high to low, the forms of protein and polysaccharide presence are transformed in the order of co-solubles, soluble complexes, insoluble complexes, soluble complexes, and co-solubles (Weinbreck et al., 2003). This effect of pH on the form of protein-polysaccharide presence is essentially a change in

* Corresponding author at: Hainan Engineering Research Center of Aquatic Resources Efficient Utilization in South China Sea, Key Laboratory of Food Nutrition and Functional Food of Hainan Province, Key Laboratory of Seafood Processing of Haikou, Engineering Research Center of Utilization of Tropical Polysaccharide Resources of MOE, College of Food Science and Technology, Hainan University, Hainan 570228, China.

E-mail address: xianguanhua@hainanu.edu.cn (G. Xia).

¹ These authors contributed equally to this study.

<https://doi.org/10.1016/j.fochx.2023.100703>

Received 28 February 2023; Received in revised form 23 April 2023; Accepted 1 May 2023

Available online 4 May 2023

2590-1575/© 2023 The Author(s). Published by Elsevier Ltd. This is an open access article under the CC BY-NC-ND license (<http://creativecommons.org/licenses/by-nc-nd/4.0/>).

the interaction forces between proteins and polysaccharides and between protein-polysaccharide complexes, where the most significant and essential force is the electrostatic interaction force (Gulao et al., 2016; Liu et al., 2015).

Whey protein isolate (WPI) is obtained from whey protein by process treatment (Santos et al., 2012). The protein content of WPI is higher than 90%, mainly including β -lactoglobulin, α -whey protein, bovine serum albumin, and other proteins, among which β -lactoglobulin and α -lactoglobulin contents are higher, and determine the functional properties of WPI (Smithers et al., 1996). WPI contains 20 kinds of amino acids, including lysine, arginine, valine, cysteine, methionine, and so on, among which the content of essential amino acids is higher than that of ordinary proteins (Morr & Ha, 1993). Typically, WPI carries a positive charge below the IEP (~5.0) (Carpentier et al., 2021) with anionic polysaccharide to form a complex. By exploiting this, complex coacervation reactions based on whey isolate proteins have been applied to the preparation of various systems, including coacervates (Sharifi et al., 2021), microcapsules (Eratte et al., 2014), edible films (Tavares et al., 2021), and powders (Tavares & Zapata Norena, 2019). Heat treatment is a common processing method in the food industry that dramatically modifies the properties of whey proteins. In view of this matter, it has also become a current challenge to broaden the application of heat-treated proteins.

Gum Arabic (GA), as a naturally anionic polysaccharide-protein complex, is widely extracted from the exudate of the trunk of the acacia tree (Patel, & Goyal, 2015). It is commonly divided into three parts: arabinogalactans, which account for about 88% of the total mass, arabinogalactan-protein, which account for about 10% of the total mass and glycoprotein, which account for about 1% of the total mass (Anderson et al., 1983). GA is claimed to show a wide range of beneficial health effects, including improving kidney function and lowering plasma cholesterol concentration (Kelley & Tsai, 1978; Lin et al., 1957). Besides, GA has been proven to be a good additive in the pharmaceutical and food industries as an emulsifier, stabilizer, and thickener (Bai et al., 2017). In previous studies, WPI and GA polymers have been extensively studied in emulsions (Roman-Guerrero et al., 2018; Yao et al., 2016), microcapsules (Bosnea et al., 2014), nanoparticles (Yao et al., 2021), and other fields, but there are few studies on their condensation mechanism, structure, and properties.

The aims of this research are to investigate the effects of heat treatment on the complex coacervations of whey isolate protein on gum arabic; to verify the combination of whey isolate protein and gum arabic by zeta potential measurement and fluorescence spectroscopy; to investigate the reaction driving forces by FTIR, intermolecular force analysis and molecular docking; and to further evaluate the changes in the structure and properties of the coacervates by X-ray diffraction (XRD), scanning electron microscopy (SEM), and differential scanning calorimetry (DSC).

2. Materials and methods

2.1. Materials

BiPro Whey protein isolate (WPI) was obtained from Davisco Foods International Inc. (Le Sueur, MN, USA), and gum Arabic (GA) was purchased from Sigma-Aldrich (Toluca, State of Mexico, Mexico). Potassium bromide (KBr), sodium chloride (NaCl), potassium chloride (KCl), calcium chloride (CaCl_2), and urea were supplied by Macklin Biochemical Technology Co. (Shanghai, China). Deionized water was used in all the experiments. Chemical reagents used in all experiments are analytically pure.

2.2. Preparation of stock solutions

GA and WPI were respectively dissolved in distilled water at room temperature and stirred continuously at 300 g for 2 h, then kept at 4°C

for another 12 h to ensure complete hydration. In addition, sodium azide (0.02%, w/v) was added to GA and WPI solutions to inhibit bacterial growth. The hWPI reservoir solution was obtained by heating the WPI solution (pH 7, 2.0% w/v) at 90 °C for 30 min and then cooling it rapidly to room temperature (Zhou et al., 2021). WPI, hWPI, and GA stock solutions (2.0% w/v) were prepared and used to study the condensation behavior of WPI-GA. The coacervate between WPI/hWPI and GA was prepared by diluting the original solution at a concentration of 0.05% (w/v) under different conditions.

2.3. Characterization of complex coacervation behavior

The influence of different environmental conditions (pH, R (WPI: GA, w/w), ionic concentration, and type) on the complex coacervation behavior was studied by turbidimetric analysis (Weinbreck et al., 2003).

Mixed solutions with different mass ratios (R: 1:3–3:1 (w/w)) were prepared by mixing two different stock solutions. The ionic strength of the mixture was adjusted with sodium chloride (0, 15, 30, and 50 mM). Then, for each mixture, the pH (6.0–1.5) was obtained by gradually dropping the hydrochloric acid solution. The concentration of the hydrochloric acid solution was gradually increased to avoid dilution of the solution system. Under certain environmental conditions, such as R, total polymer concentration, pH value, ionic strength, and type, the biopolymer stock solution was mixed and left for 2 days to prepare the solution containing the coacervate phase. The supernatant was removed and then freeze-dried for 48 h and stored at 4°C.

2.4. Turbidity measurement

The optical density (OD) of WPI solution, hWPI solution, GA solution, and their mixture was measured at 600 nm during turbidity titration. The sample was placed in a colorimetric dish and OD_{600} was recorded by UV spectrophotometer. All measurements were repeated 3 times at 25°C and expressed as mean \pm standard deviation (SD). Turbidity (τ , cm^{-1}) is defined as:

$$\tau = -\left(\frac{1}{L}\right) \ln\left(\frac{I}{I_0}\right)$$

where L is the optical path length, which is 1 cm. I is the light intensity measured by the sample, and I_0 is the light intensity of the blank control. Distilled water is used as the control in this experiment.

2.5. Zeta-potential measurement

In order to verify the formation of the complex and characterize the charge properties of the complex, the Zeta-potential (Z, mV) of WPI, hWPI, GA, and their mixtures were measured by a laser particle size analyzer. All measurements were repeated three times at 25°C (Chen et al., 2020).

2.6. Fluorescence spectral scanning

To verify the production of coagulate and explore the changes in the structure of protein coagulated with polysaccharide, the fluorescence spectra of samples were determined by an F-7100 fluorescence spectrophotometer (F-7100, Hitachi Co., Tokyo, Japan) at 25 °C. The freeze-dried samples were prepared into 0.2 mg/mL solution, and the pH was adjusted to 3.5 and 7, respectively. Then the sample solution was poured into a fluorescent colorimetric dish with an optical path of 1 cm, and the excitation wavelength and emission spectrum slit width were set to 2.5 nm. Fluorescence emission spectra in the region of 285–400 nm were collected at the excitation wavelength of 80 nm, and the endogenous fluorescence emission spectra of tyrosine and tryptophan residues were determined. Fluorescence emission spectra in the 300–400 nm region were collected at a 295 nm excitation wavelength to determine the

endogenous fluorescence emission spectra of tryptophan residues.

2.7. Scanning electron microscope (SEM)

Lyophilized samples were sectioned and sprayed with gold. Microscopic observations were performed at an acceleration voltage of 10 kV at 5000 times larger by using the S-3000N scanning electron microscope (S-3000N, Hitachi Co., Tokyo, Japan) at 25°C (Meng et al., 2021).

2.7. X-ray diffractometer (XRD)

XRD was used to determine the crystalline structure of samples after lyophilization. The crystalline structure of the combined coacervate was determined by using a SmartLab X-Ray Diffractometer (SmartLab, Rigaku, Japan). Conditions: Cu and $K\alpha$ were used for radiation, diffraction angle 2θ was scanned in the range of 5–60°, and the scanning speed was 10°/min. The operating current and voltage were 40 mA and 40 kV, respectively.

2.8. Differential scanning calorimetry (DSC)

Thermal stability was measured by using a Q100 Differential Scanning Calorimeter (Q100, TA, USA). Weigh about 4 mg of protein and the protein-polysaccharide conjugate sample into an aluminum box, compacted the aluminum box to remove air. DSC analysis parameter settings: scanning range 20–200 °C, heating rate 10 °C/min, nitrogen flow rate 20 mL/min. The universal 5.4 TA software was used to analyze the initial denaturation temperature (T_p).

2.9. Fourier transform infrared spectroscopy (FTIR)

For reducing the influence of moisture on the spectrum, especially on stretching vibration of amide I with a peptide bond, dried samples were selected for testing. 2 mg freeze-dried samples were mixed with 200 mg dried potassium bromide and ground evenly under infrared light. After being pressed into thin slices, the samples were put into Fourier transform infrared spectroscopy (FTIR-650(G), Tianjin, China) for determination (Gu et al., 2021; Hei et al., 2020). The parameters are set as follows: the scanning wavelength is 4000–400 cm^{-1} , the resolution is 4 cm^{-1} , and the scanning is 64 times. In order to eliminate the interference of non-protein components on the protein spectrum, Nicolet Omnic software (Version 8.3, Thermo Fisher Technology Co., LTD.) was used for processing, and baseline correction and deconvolution processing were performed on the samples. The amide I region (1600–1700 cm^{-1}) was most sensitive and reliable to changes in protein secondary structure.

3.10. Molecular docking

Referring to Luo et al. (2021), we investigated the interaction between WPI and Gum Arabic at the molecular level by molecular docking of β -lactoglobulin and GA. B-lactoglobulin model (6NKQ) was obtained from the NCBI database (<https://www.rcsb.org>). GA was based on the PubChem database (CID: 20728205) for construction. In this model, β -lactoglobulin is used as a p-acceptor and GA as a docking ligand.

3.11. Statistical analysis

Each experiment was repeated three times. Results are expressed as mean \pm standard deviation. Design graphics using Origin Pro 2020 software.

3. Results and discussion

3.1. Effect of pH on coacervation behavior

For characterizing the pH dependence of the coacervate reaction between WPI, hWPI, and GA solution, turbidity characteristic curves were prepared by HCl titration (Comunian et al., 2022; Liu et al., 2015; Weinbreck et al., 2003). As shown in Fig. 1A, the WPI-GA hydrochloric acid titration curve showed an overall fluctuation during the gradual decrease of the pH value. That is, the turbidity value of the solution tended to 0 at pH 6, increased slightly to 0.065 at pH 4.4, rose rapidly to a maximum at pH_{opt} (pH 3.5), and then gradually decreased until it returned to near 0. The turbidity change of the WPI, GA solution was negligible relative to the WPI-GA mixed solution.

It has been reported that the turbidity characteristic curves of protein-polysaccharides are usually divided into four phases: the first co-dissolution phase (pH_1 - pH_2), the soluble complex phase (pH_2 - pH_{opt}), the insoluble complex phase (pH_{opt} - pH_3) and the second co-dissolution phase (pH_3 - pH_{min}) (de Kruif, & Tuinier, 2001; Turgeon et al., 2007; Weinbreck et al., 2003).

As shown in Fig. 1A, the four phases of the turbidity characteristic curve of WPI-GA were: in the first co-soluble phase (pH 6.0 ~ pH 5.5), the solution turbidity was almost 0; in the soluble complex phase (pH 5.5 ~ pH 5.0), the solution turbidity increased slightly; in the insoluble complex phase (pH 5.0 - pH 2.2), the solution turbidity first increased sharply (pH 5.0 - pH 4), reaching a maximum at pH 4 and then gradually decreasing (pH 4-pH 2.2); in the second co-soluble phase (pH below 2.2), the turbidity value of the solution tends to 0 again. Weinbreck et al. (2004) in their study used pH 4 as the optimum pH for WPI-GA (R = 2:1) coalescence of the encapsulated oil phase. but, the present study concluded that WPI-GA possessed the maximum degree of binding at pH 3.5. This may be due to the change in the components of WPI. As shown in Fig. 1B, similarly, the pH-turbidity characteristic curve of hWPI-GA can be divided into four stages. In the first co-soluble phase (pH 6.0 - pH 5.5), the turbidity value of hWPI-GA is almost 0. In the soluble complex phase (pH 5.5 - pH 5.0), the turbidity increases slightly to 0.029. In the insoluble complex phase (pH 5.0 - pH 2.2), the turbidity first increased sharply (pH 5.0 - pH 4), reaching a maximum value of 1.001 at pH 4, and then gradually decreased (pH 4 - pH 2.2), returning to 0.023 at pH 2.2. In the second co-soluble phase (pH below 2.2), the turbidity value of the solution again tends to be 0.

3.2. Effect of pH on charged properties

The pH determines the degree of ionization of the amino and carboxyl groups possessed by WPI and the acidic groups carried by GA. In GA, the acidic sugar chains attached to the protein provide a large amount of negative charge (Comunian et al., 2022). The main component of WPI is β -lactoglobulin, which contains a large number of anionic and cationic residues that provide a large amount of negative and positive charge to WPI (Jones et al., 2010). As the pH decreases, the WPI is gradually protonated, leading to a change in the WPI-GA binding state.

The Zeta-potential curves for all sample solutions are shown in Fig. 2A. For the WPI-GA mixed solutions, from pH 6 to pH 5, both WPI and GA had high negative charges (−23.7 mV and −36.96 mV). This demonstrated that all proteins and polysaccharides have a strong electrostatic repulsion to resist mutual aggregation. Similar results were obtained in the report by Gulao et al. (2016) about the peptide leucine and gum arabic. From pH 5 to pH 4, the Zeta potential of the WPI-GA mixed solution decreased from −23.03 mV to −10.33 mV. The positively charged groups on the surface of WPI gradually combined with the negatively charged groups of GA to form soluble complexes before the pH dropped to 4.4. The soluble complexes in this process had enough negative charges on their surfaces, and the electrostatic repulsion between them was sufficient to resist aggregation, so the turbidity of the mixed solution only increases slightly. After the pH value dropped to

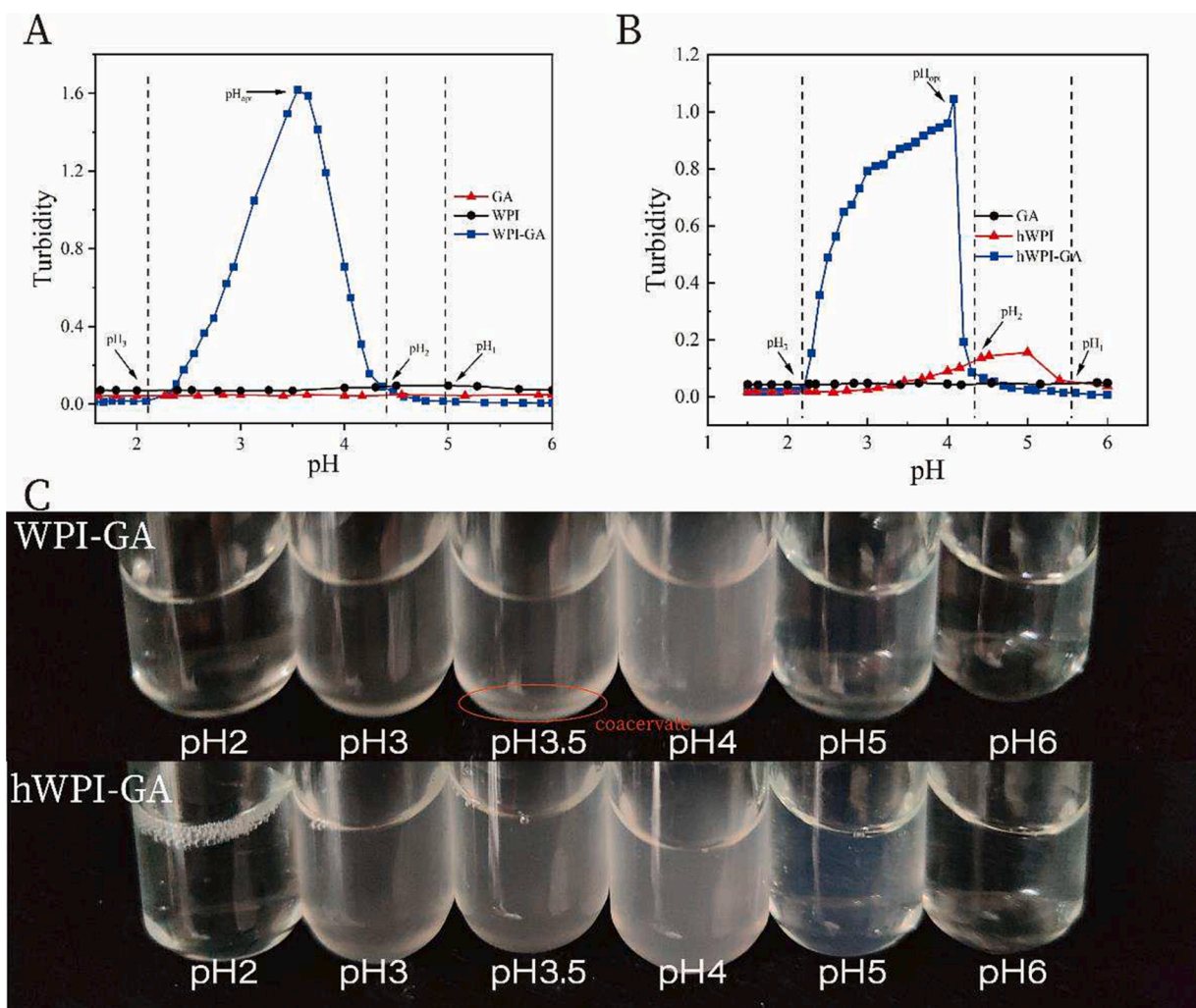


Fig. 1. Turbidity curves of WPI-GA (A) and hWPI-GA (B) and photographs of the mixed solutions (C).

4.4, the net negative charge on the surface of soluble complexes further decreased and the electrostatic repulsive force decreased, leading to the conversion of soluble complexes into insoluble ones. From pH 4.0–pH 3.0, the Zeta potential of the WPI-GA complex solution decreased from -10.33 mV to -6.44 mV. The isoelectric point of the WPI-GA complex (located around pH 3.5) during this phase just corresponds to the pH_{opt} of WPI-GA. At pH 3.5, the electrostatic repulsion between the WPI-GA complexes reached its lowest, leading to the highest turbidity values. From pH 3.0 to pH 2.0, the Zeta potential of the WPI-GA complex solution decreased from 6.44 mV to 3.70 mV. The zeta potential of WPI was as high as (39.20 mV – 34.10 mV) and the zeta potential of GA was -15.96 mV to -0.82 mV. The electrostatic attraction between WPI and GA was gradually weakening, and therefore the degree of binding between the two was gradually decreasing. This led to the final solution with almost no change in turbidity in the second co-solubilization phase ($pH 2.2 - pH_{min}$).

A similar phenomenon appeared in the Zeta potential curves of the hWPI-GA mixture solution. However, the difference was that hWPI had a higher negative charge (-33.4 mV) at pH 6, which reveals that WPI exposes more anionic groups after heat treatment. Moreover, the isoelectric point of hWPI-GA was altered, which may be the reason why hWPI-GA has a different complex coacervation behavior from that of WPI-GA.

3.3. Fluorescence spectrum

Fluorescence spectroscopy has been widely accepted to detect changes in protein structure. At different excitation and emission wavelengths, the changes in protein structure can be characterized by the fluorescence features of the fluorescent moieties. To verify the formation of coacervate and to further explore the effect of condensation reactions on protein structure, the fluorescence characteristics were examined by fluorescence spectroscopy.

The fluorescence spectra obtained are shown in Fig. 2BC and Fig. S1. First of all, the fluorescence intensity of the GA can be detected at lower levels (Liu et al., 2022) for both 280 nm and 295 nm excitation wavelengths, but is well below the WPI and can be negligible at pH 3.5 and pH 7 conditions. At the excitation wavelength of 280 nm, the fluorescence intensity of the mixed solution was slightly reduced after the addition of GA (pH 7.0); after the addition of GA (pH 3.5), the fluorescence intensity of the mixed solution was substantially reduced. The same phenomenon was observed for the excitation wavelength of 295 nm. This shows that the added GA combines strongly with WPI at pH 3.5, but the hydrophobic environment where tyrosine and tryptophan residues are located is not significantly improved. It is commonly believed that after adding polysaccharides, some tryptophan residues are encapsulated within other macromolecular side chains through protein–protein and protein–polysaccharide molecule interactions (Niu et al., 2015). A similar phenomenon was observed by Luo et al. (2021). After the addition of gum Arabic (pH 3.0), the fluorescence intensity of rice glutenin gradually

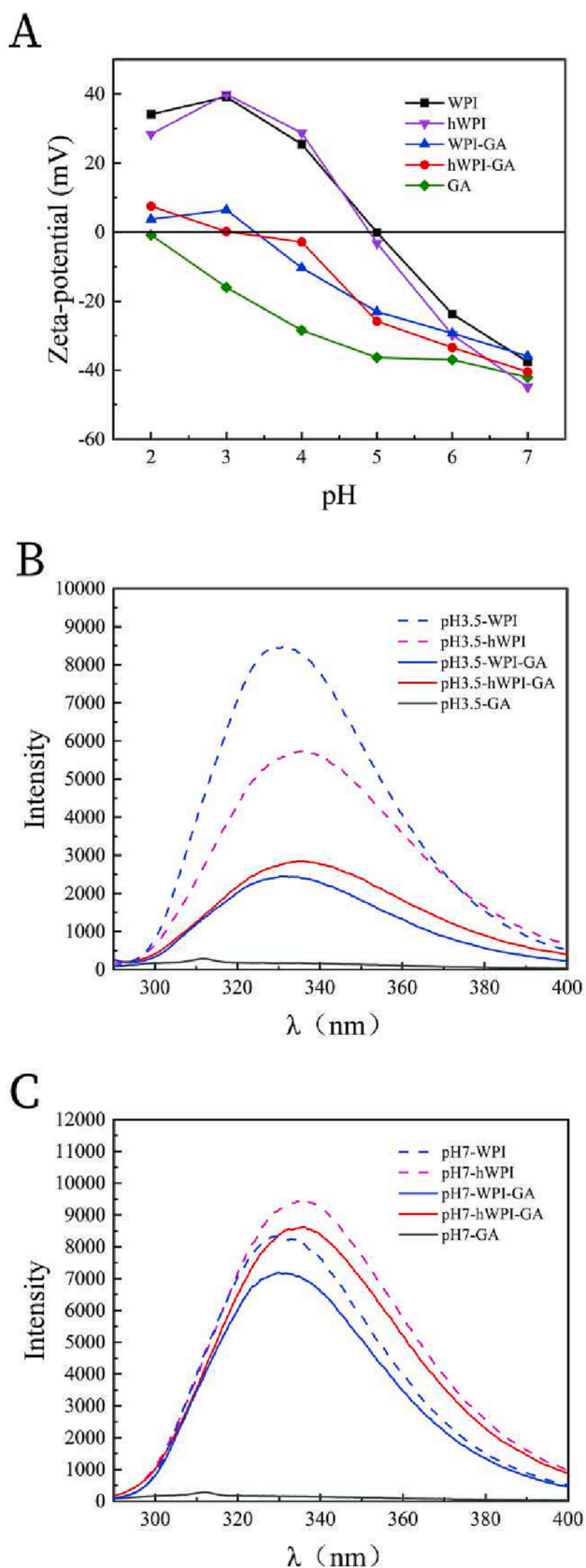


Fig. 2. Zeta-potential curves for samples (A) and the fluorescence spectra of the mixed solution at pH 3.5 (B) and pH 7 (C) (excitation wavelength 280 nm).

decreased without significant changes in λ_{\max} , and the RG-GA complex formed as a static burst.

A similar phenomenon occurred in the mixture of hWPI and GA. Besides, the λ_{\max} of the hWPI solution showed a significant shift. At the 280 nm excitation wavelength, the λ_{\max} of hWPI shifted from 331 nm to 338 nm at pH 3.5 and from 331 nm to 337 nm at pH 7. At the 295 nm excitation wavelength, the λ_{\max} of hWPI shifted from 331 nm to 336 nm at pH 3.5 and pH 7. The maximum emission wavelength redshift indicated that the tryptophan residue is in an environment with enhanced polarity and hydrophilicity. This result suggests that heat treatment changes the spatial structure of WPI to expose internal amino acid molecules. This result indicated that WPI/hWPI combined with GA in a form where the protein was located medially and GA was located laterally. Moreover, affected by heat treatment, hWPI exposed more amino acid groups, consistent with the enhanced zeta potential.

3.4. Analysis of the driving forces behind coacervation behavior

As mentioned above, the protein-polysaccharide complex coacervation reaction is driven by a variety of non-covalent forces such as hydrophobic interaction, electrostatic interaction, and the hydrogen bond. Some chemical dissociation agents (including NaCl, urea, and DTT) can affect these forces. Thus, the driving forces for the reaction of WPI/hWPI with GA can be analyzed in more detail using these properties (Liu et al., 2015). According to Li et al. (2016), we use a simplified procedure to explore the main intermolecular non-covalent forces in the formation of coacervate.

NaCl works as a dissociating agent to reduce electrostatic interactions by shielding the cationic and anionic groups on the surface of biomolecules. Fig. 3A shows the turbidity curves with and without the addition of NaCl. The turbidity curve for NaCl at 100 mM showed almost no fluctuations and therefore was not shown. The turbidity of the mixed solutions at different pH values decreased significantly after the addition of NaCl. In addition, the maximum turbidity of the mixed solutions decreased successively with the increase in NaCl addition. The result demonstrates that electrostatic interactions are an important driving force for the coacervation behavior of the WPI-GA and hWPI-GA complexes.

Urea is frequently used as a reagent that interferes with hydrogen bonding or hydrophobic interactions (Yan et al., 2020). The complex cohesive behavior of protein-polysaccharides is influenced by electrostatic interactions as well as hydrophobic interactions (Rocha et al., 2014). Fig. 3B showed the turbidity curves at different concentrations of urea. The addition of urea reduced the turbidity of all mixed solutions at different pH values. According to Kirkwood Buff theory, it is known that the accumulation of urea molecules around the hydrophobic groups of proteins, especially in the side chains of amino acids with high molecular weight, generates a forward transfer ΔH through its temperature dependence, which disrupts the hydrophobic interaction between proteins and polysaccharides (Shimizu, 2011). This suggested that hydrogen bond breaks and hydrophobic interactions between the protein and polysaccharide were disrupted during the coacervation reaction, leading to a small dissociation of the self-assembly behavior between the protein and the polysaccharide. Compared to NaCl, urea caused less damage to the complex structure in the complex coacervation reaction. GA contains a large number of acidic groups (such as glucuronic acid) (Comunian et al., 2022). WPI contains a large number of anionic and cationic residues, which provide a large number of action targets for Na^+ and Cl^- . In addition, the contact angle test shows that WPI/hWPI, GA has a high hydrophilicity ($<90^\circ$) under acidic conditions, which makes the action target of urea less. The results suggested that electrostatic interactions were the main driving force.

3.5. Effect of biopolymer ratio on coacervation behavior

From the observation in Fig. 3CD, it was evident that as the WPI/GA

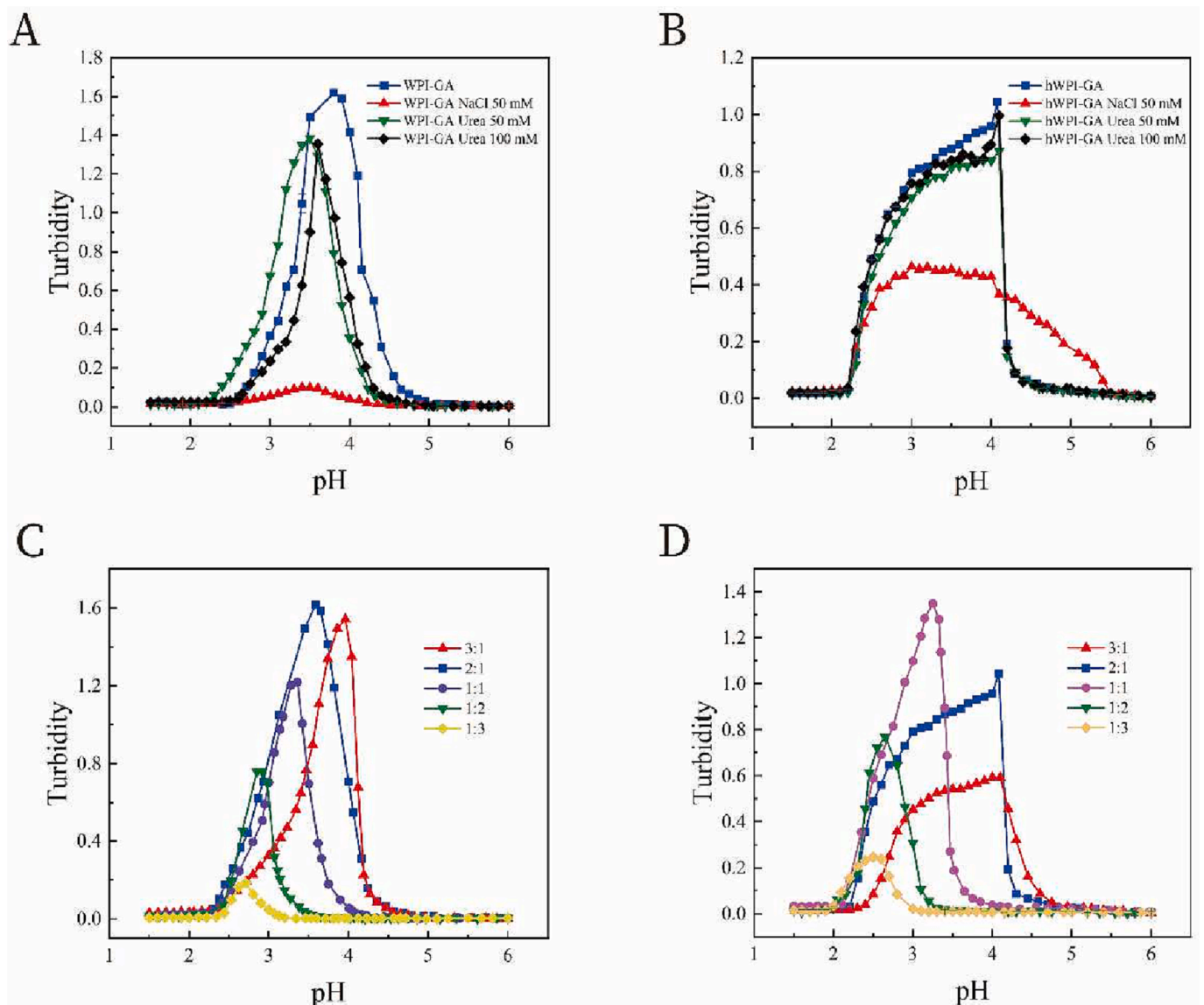


Fig. 3. Turbidity curves of WPI-GA (A) and hWPI-GA (B) with different concentrations of NaCl and Urea; turbidity curves of WPI-GA (C) and hWPI-GA (D) under different biopolymer ratios.

ratio (R) gradually increased, the maximum turbidity value decreased gradually and the key pH points moved towards an acidic environment.

When R was transformed from 3:1 to 1:3, pH_1 shifted from pH 5.60 to pH 3.34, pH_2 shifted from pH 5.00 to pH 3.07, pH_{opt} shifted from pH 4.40 to pH 2.71, and pH_3 was maintained at about pH 2.20 (Fig. S2). At R below 2:1, the protein was shielded by excess GA, resulting in a decrease in the maximum turbidity value. At R higher than 2:1, GA was saturated with protein. Therefore, the maximum turbidity of the WPI-GA complex solution was obtained at R = 2:1.

The optimal ratio of WPI/GA combination has been controversial. In the study of Eratte et al., (2014), 3:1 was considered as the optimal ratio for WPI-GA complexation. Unlike the present study, it was found that a more intense degree of WPI-GA binding was obtained at pH 3.5 with R = 2:1. Similar results were found by Niu (Niu et al., 2015). This may be due to the poor light-scattering properties of the gum arabic molecule itself. As the ovalbumin/gum arabic ratio increased from 1:1 to 24:1, the turbidity curves shifted to higher pH values, achieving maximum turbidity values at a ratio of 2:1. Liu et al. (2009) also showed similar results in the study of pea isolate and Arabic gum. Based on these studies, it can be found that WPI-GA, OVA-GA, and PPI-GA exhibit similar complex coagulation behavior after using the same

polysaccharides, that is, the maximum turbidity value is reached at R = 2:1. In contrast, hWPI exhibited a different reconcondensation behavior. The reason for this was probably that after heat treatment, hWPI exposed more charged groups, resulting in more binding sites (mainly cationic groups) on the surface than WPI. The hWPI thus took less than the WPI to saturate with adsorption when the amount of GA was equal. For comparison purposes, R = 2:1 was adopted for the subsequent study.

3.6. Effect of ionic types and concentrations on coacervation behavior

Based on the above analysis of the complex coacervation drivers, it is evident that ion type and concentration have an important effect on the complex coacervation behavior. To research the effect of ion type and strength on the complex coacervation behavior, the turbidity curves of the mixed solutions containing different NaCl concentrations and different ion types (NaCl, KCl, $CaCl_2$) were characterized. As shown in Fig. 4A, as the NaCl concentration increased from 0 to 50 mM, the maximum turbidity of the WPI-GA mixture decreased from 1.618 to 0.097 and the maximum turbidity of the hWPI-GA mixture decreased from 1.001 to 0.44. In general, NaCl combines with negatively and positively charged groups on GA and WPI in solution in the form of Na^+

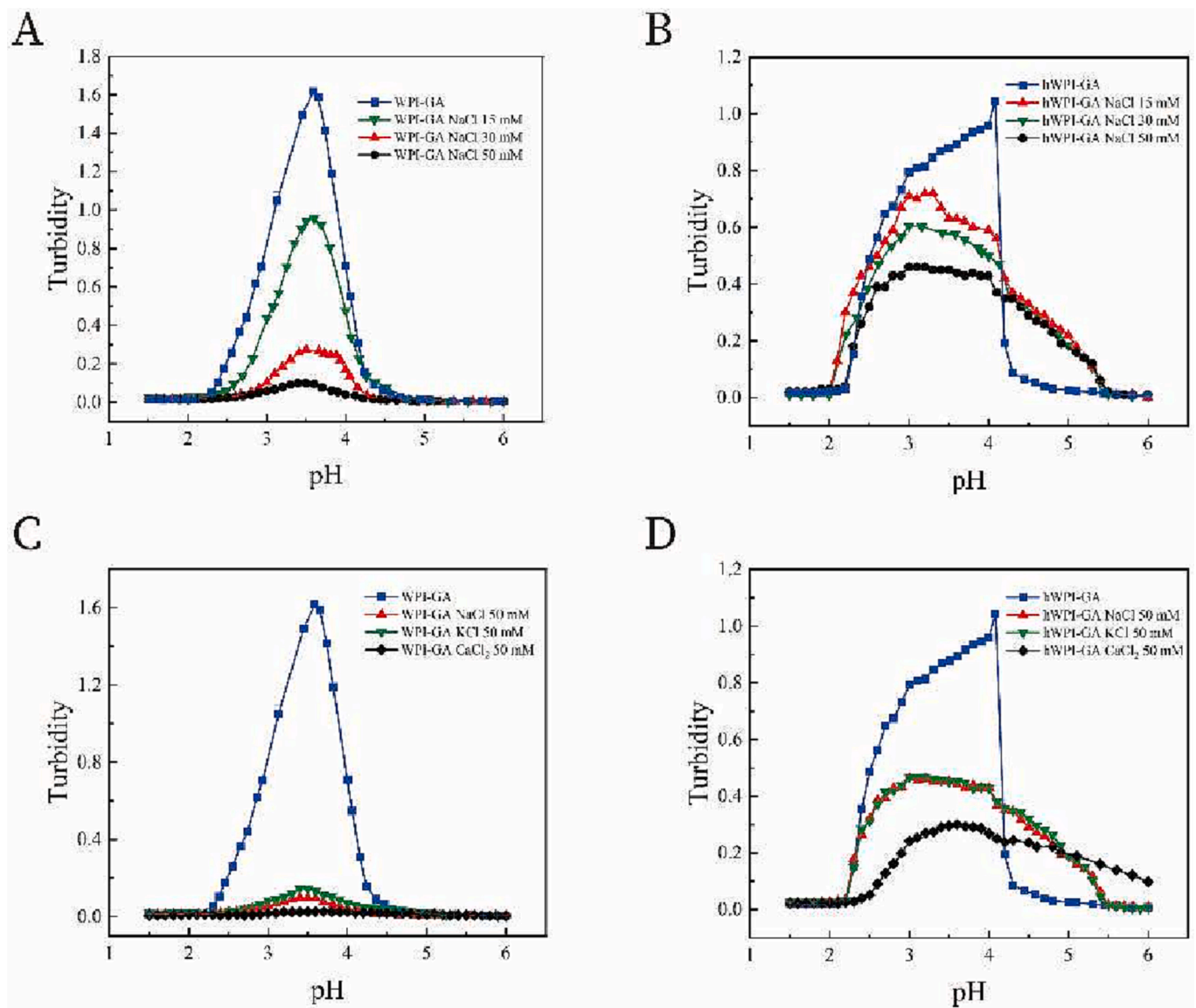


Fig. 4. Turbidity curves of WPI-GA (A) and hWPI-GA (B) with different ion types and WPI-GA (C) and hWPI-GA (D) with different NaCl concentrations.

and Cl^- , leading to a reduction in the binding sites between proteins and polysaccharides (Luo et al., 2021; Yan et al., 2020). The complex coacervation behavior of WPI/hWPI with GA is affected by the concentration and type of salt ion, which is attributed to its entropic effect with changes in Coulomb interactions. For pure proteins, salt ions reduce the charge on the protein by binding to it, thus reducing the energy barrier for precipitation, and divalent cations significantly accelerate the aggregation process by increasing the accumulation around the intermediate state during aggregation (Harton and Shimizu, 2019). In the range of strong Coulombic interactions of highly charged polymers, the enthalpy of complexation is weakly dependent on the salt concentration, and the counterion release entropy varies greatly with salt concentration, so that complexation between this polymeric electrolyte is driven by a large counterion release entropy (Ou, & Muthukumar, 2006). The higher the concentration of NaCl, the higher the content of Na^+ and Cl^- , and the weaker the degree of binding between proteins and polysaccharides.

According to Fig. 4CD, the addition of KCl did not significantly change the pH_{opt} and turbidity maximum of the mixed solution compared to the mixed solution containing NaCl. Although Na^+ and K^+ were different cations, they both carried a positive charge and had a

similar attraction to the anionic groups on the surface of proteins and polysaccharides. As such, the turbidity curves obtained after the addition of NaCl and KCl were similar. The results show that ions at the same price had similar effects on the complex coacervation process. For the mixed solution of WPI-GA, the maximum turbidity value of the solution containing CaCl_2 was significantly lower than that of the one containing NaCl at the same concentration. Compared with monovalent cations such as Na^+ and K^+ , Ca^{2+} loses two electrons and has a stronger competitive ability to bind to acidic groups on GA than positively charged groups such as Na^+ , K^+ , and amino groups on WPI (Niu et al., 2015). The difference was that the addition of CaCl_2 increased the turbidity of the hWPI-GA solution (from the initial stage). This indicated that the hWPI-GA complex coacervation behavior had a lower ionic tolerance than that of the WPI-GA.

3.7. Effect of total polymer concentration on coacervation behavior

To evaluate the effect of total biopolymer concentration on the complex coacervation behavior of WPI/hWPI and GA, the turbidity curves of total polymer concentration in the range of 0.025–0.1 wt% were studied. As can be seen from Fig. 5 and S3, with the decrease in the

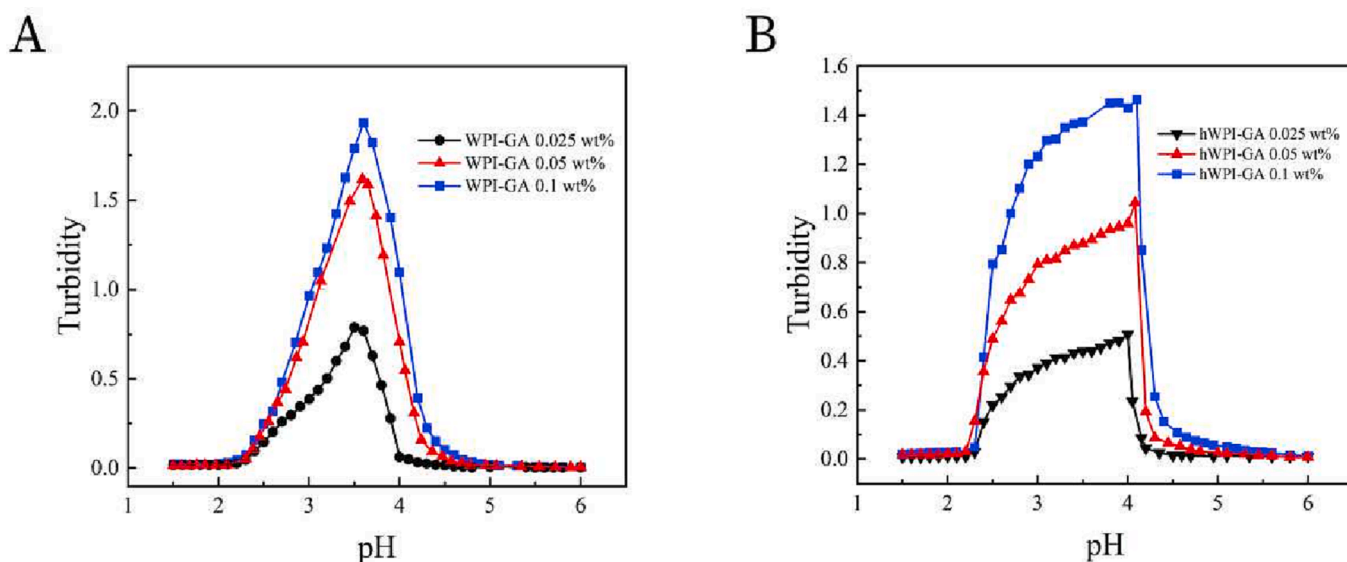


Fig. 5. Turbidity curves of WPI-GA (A) and hWPI-GA (B) under different biopolymer concentrations (0.025, 0.05, and 0.1 wt%).

total polymer concentration, the maximum turbidity value of the WPI/GA mixture decreased, and the critical pH point shifted towards acidity. As the total polymer concentration decreased from 0.1 wt% to 0.025 wt%, pH_1 of the WPI-GA complex coacervation reaction shifted from pH 5.6 to pH 4.8, pH_2 from pH 4.4 to pH 4.0, and pH_{opt} from pH 3.6 to pH 3.5; pH_1 of the hWPI-GA complex coacervation reaction shifted from pH 5.8 to pH 4.7, pH_2 from pH 4.55 to pH 4.2. As the total polymer concentration of the mixed solution decreased, the maximum turbidity value of the WPI/GA mixture decreased from 1.933 to 0.787 and the maximum turbidity value of the hWPI/GA mixture decreased from 1.463 to 0.507. Additionally, the growth rate of the maximum turbidity gradually decreased with increasing total polymer concentration.

Daoub et al. (2018) concluded that the decrease in coacervation rate during the increase in total biopolymer concentration resulted from the release of Na^+ , Ca^{2+} , and Cl^- . The ions isolated the relatively charged complexes and increased the mutual solubility of the coacervate and equilibrium solution phases. Interestingly, the shift of the critical pH point in the WPI-GA complex coacervation reaction was similar to the effect of low-concentration ions on the turbidity profile of the WPI-GA mixed solution, which can be explained as caused by ions released from biomolecules. But the difference was that the sensitivity of the hWPI-GA complex coacervation reaction to low concentrations of ions

was not reflected in the increase in the total polymer concentration. We speculated that the slowdown in the rate of increase of the maximum turbidity value as the total biopolymer concentration increased was not only related to the anti-equilibrium ions but also to the spatial blocking effect between biomacromolecules.

3.8. Structure observation of coacervate

The microstructure was obtained by SEM scan as shown in Fig. 6A. While WPI on its own had a uniform structure, WPI-GA coacervate was observed to have a three-dimensional gel mesh structure. Unlike the lamellar structure of WPI, WPI-GA coacervate showed a typical gel-like structure, which was consistent with its gel-like appearance (Dong et al., 2022; Liu et al., 2020). Microgel particles can be observed in hWPI (Dong et al., 2022). The hWPI-GA had a loose appearance, and the microstructure of the coacervate appears as a loose mesh. hWPI-GA consisted of particles, which may be related to the fact that hWPI has a spherical structure. These results were in agreement with the turbidity curves and fluorescence spectroscopy results, further confirming that WPI/hWPI complexes with GA through interactions and that the coacervates have different structures. The structure of the protein-polysaccharide coacervates depends on their nature. Rocha et al.

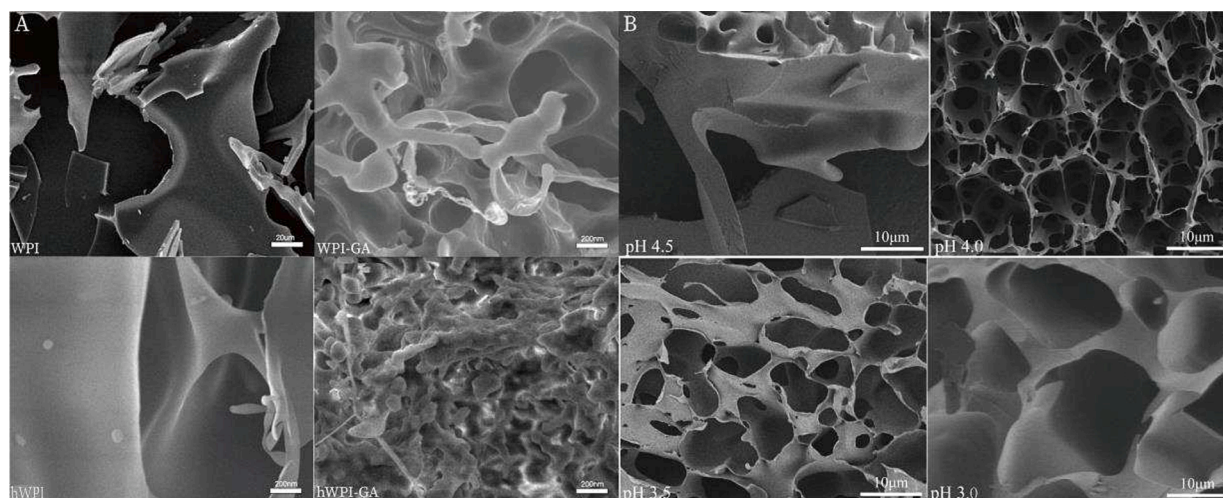


Fig. 6. Microstructures of WPI-GA coacervate, hWPI-GA coacervate (A), and WPI-GA coacervate at different pH (pH 4.5, 4.0, 3.5, 3.0) (B).

(2014) revealed that the increase of the acidic group of the polysaccharide prompted the coacervates to behave as blocky precipitates, attributed to the stronger attraction of the amine group of the protein to the sulfate group than to the carboxylic acid group. From the present study, it is clear that the coacervates appear as bulk precipitates despite the absence of a significant increase in the net positive charge of hWPI under acidic conditions. This may be attributed to the simultaneous increase in the exposure of protein anionic and cationic residues after heat treatment. Although the net charge of hWPI was maintained in relative equilibrium under this treatment, the charge density of hWPI increased and the binding to GA was enhanced, resulting in the formation of low hydrated coacervates. In summary, due to the loose appearance and sparse mesh of the hWPI-GA coacervate, the WPI-GA coacervate was collected and investigated..

The formation process of WPI-GA coacervate was visualized (Fig. 6B). At pH 4.5, WPI-GA showed a homogeneous structure with fewer mesh pores; at pH 4.0, WPI-GA showed a porous structure with weak walls; at pH 3.5, WPI-GA showed a structure with thick pore walls and dense mesh pores; at pH 3.0, WPI-GA showed a thick, loose mesh pore. These results are consistent with the results of turbidity curves and potential curves of WPI-GA, further demonstrating that pH affects the structure of WPI-GA coacervates by changing the strength of the interaction force between WPI and GA.

3.9. FTIR

The FTIR spectra of WPI, GA and, WPI-GA coacervate freeze-dried samples were shown in Fig. 7A. Noticeably, the spectra of WPI exhibited a characteristic absorption peak at 3427 cm^{-1} related to $-\text{OH}$ contraction vibrations, associated with hydrogen bonding (Zhou et al., 2022). There was a characteristic peak at 1636 cm^{-1} belonging to the amide I band ($1600\text{--}1700\text{ cm}^{-1}$), attributed to $\text{C}=\text{O}$ stretching vibration, at 1590 cm^{-1} according to the amide II band ($1450\text{--}1600\text{ cm}^{-1}$), due to $\text{N}-\text{H}$ stretching combination, with characteristic peaks at 1362 cm^{-1} and at 1238 cm^{-1} in the amide III band ($1400\text{--}1200\text{ cm}^{-1}$), which were attributed to $\text{C}-\text{N}$ stretching and $\text{N}-\text{H}$ bending.

In contrast, The spectrum of GA showed a characteristic absorption peak at 3405 cm^{-1} , which was generated by $-\text{OH}$ and $\text{N}-\text{H}$ stretching vibrations (Daoub et al., 2018). The peaks at 1611 cm^{-1} and 1419 cm^{-1} in the FTIR spectrum represent the stretching and asymmetric vibrations of $-\text{COO}^-$. The WPI-GA coacervates were significantly different from the structures of both WPI and GA. Compared with WPI, WPI-GA coacervate also had characteristic peaks at 3427 cm^{-1} , 1636 cm^{-1} , 1590 cm^{-1} , and 1362 cm^{-1} , but the absorption peak at 1238 cm^{-1} disappeared and the intensity of each peak decreased. Compared with GA, the WPI-GA coacervate lacks absorption peaks at 1611 cm^{-1} and 1419 cm^{-1} . This phenomenon suggested that WPI interacts with GA through electrostatic interactions, making the $-\text{NH}_3^+$ of WPI and the $-\text{COO}^-$ group of gum arabic canceled out. The results of this phenomenon were consistent with the FTIR spectra of ovalbumin and propylene glycol alginate coacervate (Zou et al., 2020). This result was consistent with the data of zeta potential, fluorescence spectra, and intermolecular force analysis, indicating that WPI and GA were combined mainly through electrostatic interactions to form a WPI within and GA outside complex structure. Similar results appeared in the study of Plati and Paraskevopoulou (2023), but it is interesting that the signal peak representing electrostatic interactions in this WPI-GA coacervate did not disappear completely, which may be related to the different compositions of WPI. β -lactoglobulin tended to form a complex with GA at pH 4.5, and α -lactalbumin tended to form a complex at pH 3.5. As the β -lactoglobulin/ α -lactalbumin ratio of WPI changed, the FTIR spectral structure of WPI-GA also changed.

3.10. XRD

Fig. 7B showed the X-ray diffraction curves of WPI, GA, and their

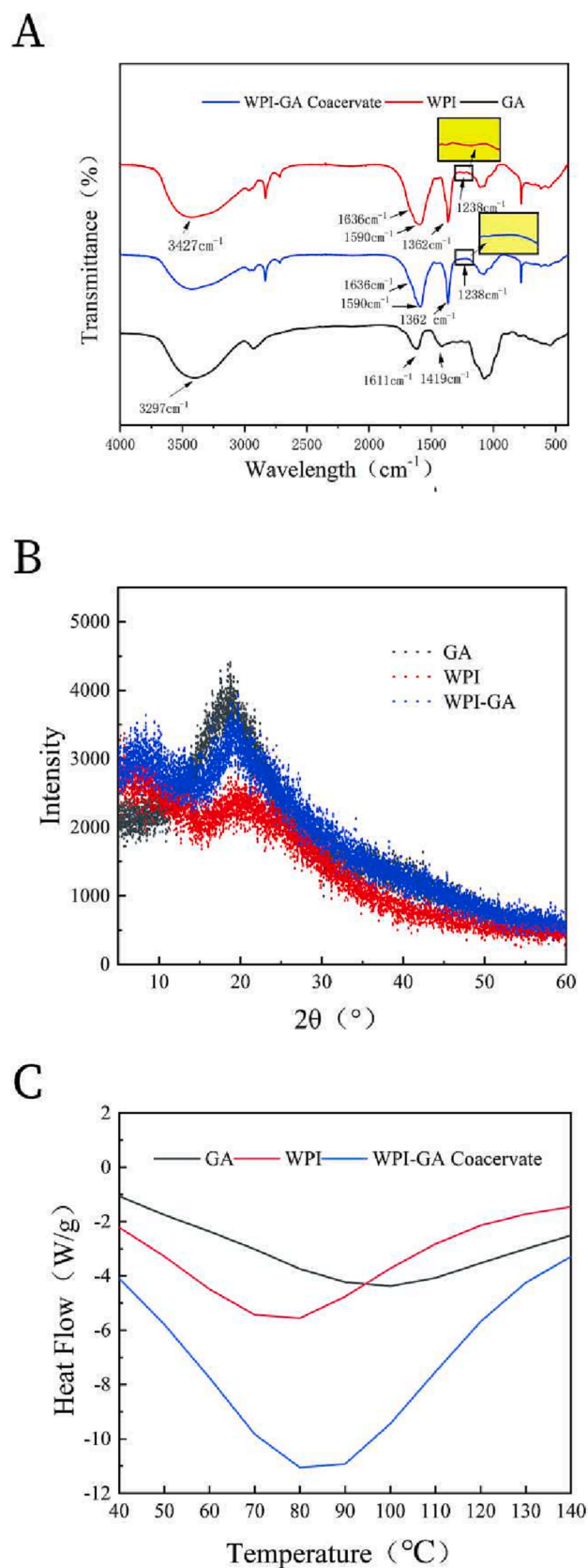


Fig. 7. FTIR (A), XRD (B), and DSC (C) results of WPI, GA, and WPI-GA coacervate.

coacervate. Two wide peaks were observed in WPI (7.53° and 10.56°), indicating the presence of crystal regions and non-covalent bonds in the WPI. One peak was observed in WPI (18.46°) (Gulao et al., 2016). In contrast, the WPI-GA coacervate showed similar peaks at the same position in the curve of WPI (7.53° and one at 10.56°), which indicated the existence of WPI in the coacervate and retained the amorphous property of WPI (Baeza, & Pilosof, 2002). In addition, the diffraction peak intensity of the coacervate was significantly higher than that of WPI alone, indicating that the crystallinity of WPI-GA coacervate is strengthened. Zou et al. (2020) also obtained a similar structure in the complex coacervate of ovalbumin-propanediol alginate, which may be due to the rearrangement of proteins and polysaccharides to form larger coacervate after the interaction.

3.11. DSC

WPI contains a large amount of globular protein. During heat treatment, WPI absorbs thermal energy and opens its spatial structure, exposing its internal groups. This changes the physical and chemical properties of the WPI, resulting in the aggregation of denatured proteins with each other to form protein polymers (Baeza et al., 2002). Therefore, DSC can be applied to monitor changes in protein denaturation temperature (T_p) to assess its thermal stability (Liu et al., 2020; Tavares et al., 2021).

The DSC heating curves of WPI, GA, and their coacervate were shown in Fig. 7C. All samples showed a similar endothermic peak over a wide temperature range. The T_p of WPI samples was 80.13°C, which corresponds to the thermal denaturation of β -lactoglobulin and was consistent with Baeza et al. (2002). The T_p of GA appears at 95.92°C, which meant that GA had better heat resistance than WPI. This may be because GA had a larger molecular weight and more stable polysaccharide chains than proteins. Furthermore, the T_p of the WPI-GA coacervate appears at 88.51 °C and the peak was larger than that of WPI, which suggested that the expansion of the spatial structure of the WPI-GA coacervate required higher temperature and heat than that of WPI. This also implied that the thermal stability of WPI-GA coacervate is superior to that of WPI. Tavares et al. (2021) reported the corresponding conclusion. At pH 6, the T_p value of β -lactoglobulin was elevated after combining with k-carrageenan, xanthan gum, and propylene glycol alginate. Combined with the results of fluorescence spectroscopy scan, it can be seen that the increase of thermal stability of WPI-GA coacervates may be due to the presence of WPI-GA coacervates in a binding morphology with WPI at

the core and GA at the outside, and GA retards the denaturation of internal WPI with a high reduction of spatial potential resistance.

3.12. Molecular docking

Molecular docking was used to further explore the interaction of WPI with GA. Since the major protein of WPI is β -lactoglobulin, the β -lactoglobulin model in an acidic environment was used to perform this computational simulation. As shown in Fig. 8A, GA is bound on the surface of the protein. β -lactoglobulin has 15 amino acid residues that interact with GA (Val 128, Asn 152, Pro 153, Phe 151, His 146, Ser 150, Leu 133, Met 145, Ala 25, Arg 148, Asp137, Leu 143, Leu 140, Lys 141, Pro 144). Among them, most of the amino acid residues (Lys 141, Asp 147, Leu 143, Leu 133, Ala 25, Pro 153, Ser 150, Asn 152) are bound to GA by van der Waals forces. Also, a small number of hydrophobic interactions (Leu 140 (2.84 Å), Met 145 (2.60 Å)), Pi-cation (His 146 (3.66 Å)), Pi-Pi T-shaped (Val 128 (4.58 Å)) and other forces were present between β -lactoglobulin and GA. The results of molecular docking are similar to those of intermolecular forces, FTIR, and Zeta. This indicated that electrostatic interactions are the main driving force to drive the binding of WPI to GA on a molecular scale.

4. Conclusion

In this work, coacervate was formed at a mass ratio of 2:1 and a pH 3.5. The results of fluorescence spectroscopy confirm this and reveal that the polysaccharide is located on the outer side of the protein in the structure of the complex. Heat treatment increased the surface charge of WPI, reduced the saturated adsorption concentration of GA, and enhanced the sensitivity of the complex coacervation reaction to divalent ions. With the increase in salt ion price, the increase in salt ion concentration, and the decrease in total biomacromolecule concentration, the maximum turbidity of the complex coacervation reaction decreased. The intermolecular force analysis and molecular docking results reveal that electrostatic forces remain the main driving force for the coacervation behavior of whey isolates complexed with GA. FTIR and intermolecular force analysis confirmed that the coacervate with or without heat treatment, was formed as a result of electrostatic interactions. From the SEM and DSC results, it is clear that the whey isolate protein combined with gum arabic forms a gel-like coacervate with higher thermal stability and a dense structure. This study provides more in-depth theoretical guidance for the application of the complex

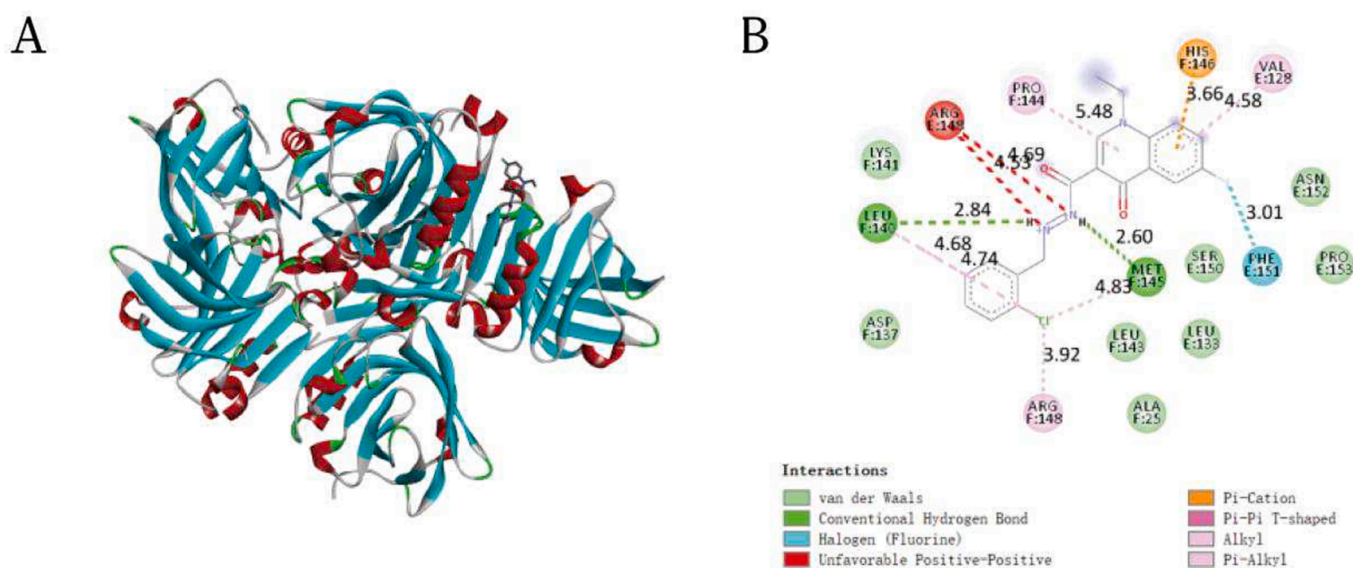


Fig. 8. Molecular docking of β -lactoglobulin and GA (A), and binding sites for β -lactoglobulin and GA interactions (B).

coacervation reaction of WPI with polysaccharides.

CRedit authorship contribution statement

Xiaoshan Wan: Conceptualization, Methodology, Data curation, Investigation, Software, Visualization, Formal analysis, Writing – original draft. **Meihui Zhao:** Conceptualization, Methodology, Investigation, Formal analysis, Writing – review & editing, Supervision. **Mengxue Guo:** Conceptualization, Methodology, Writing – review & editing, Supervision. **Peng Li:** Conceptualization, Writing – review & editing, Supervision. **Haohao Shi:** Conceptualization, Writing – review & editing. **Xueying Zhang:** Conceptualization, Writing – review & editing. **Zhongyuan Liu:** Conceptualization, Supervision. **Guanghua Xia:** Conceptualization, Resources, Writing – review & editing, Funding acquisition, Supervision, Project administration, Resources.

Declaration of Competing Interest

The authors declare that they have no known competing financial interests or personal relationships that could have appeared to influence the work reported in this paper.

Data availability

Data will be made available on request.

Acknowledgements

This work was supported by National Natural Science Foundation of China (No. 31860450).

Appendix A. Supplementary data

Supplementary data to this article can be found online at <https://doi.org/10.1016/j.fochx.2023.100703>.

References

- Anderson, D. M. W., Bridgeman, M. M. E., Farquhar, J. G. K., & McNab, C. G. A. (1983). The chemical characterization of the test article used in toxicological studies of gum arabic (*Acacia senegal* (L.) Willd). *International Tree Crops Journal*, 2(3–4), 245–254. <https://doi.org/10.1080/01435698.1983.9752758>
- Baeza, R. I., & Pilosof, A. M. R. (2002). Calorimetric studies of thermal denaturation of β -lactoglobulin in the presence of polysaccharides. *LWT – Food Science and Technology*, 35(5), 393–399. <https://doi.org/10.1006/food.2001.0862>
- Bai, L., Huan, S., Li, Z., & McClements, D. J. (2017). Comparison of emulsifying properties of food-grade polysaccharides in oil-in-water emulsions: Gum arabic, beet pectin, and corn fiber gum. *Food Hydrocolloids*, 66, 144–153. <https://doi.org/10.1016/j.foodhyd.2016.12.019>
- Bosnea, L. A., Moschakis, T., & Biliaderis, C. G. (2014). Complex coacervation as a novel microencapsulation technique to improve viability of probiotics under different stresses. *Food and Bioprocess Technology*, 7(10), 2767–2781. <https://doi.org/10.1007/s11947-014-1317-7>
- Cabezas, D. M., Pascual, G. N., Wagner, J. R., & Palazolo, G. G. (2019). Nanoparticles assembled from mixtures of whey protein isolate and soluble soybean polysaccharides. Structure, interfacial behavior and application on emulsions subjected to freeze-thawing. *Food Hydrocolloids*, 95, 445–453. <https://doi.org/10.1016/j.foodhyd.2019.04.040>
- Carpentier, J., Conforto, E., Chaigneau, C., Vendeville, J.-E., & Maugard, T. (2021). Complex coacervation of pea protein isolate and tragacanth gum: Comparative study with commercial polysaccharides. *Innovative Food Science & Emerging Technologies*, 69, Article 102641. <https://doi.org/10.1016/j.ifset.2021.102641>
- Chen, L., Shen, X. R., & Xia, G. H. (2020). Effect of molecular weight of tilapia (*Oreochromis niloticus*) skin collagen peptide fractions on zinc-chelating capacity and bioaccessibility of the zinc-peptide fractions complexes in vitro digestion. *Applied Sciences-Basel*, 10(6), 11. <https://doi.org/10.3390/app10062041>
- Comunian, T. A., Archut, A., Gomez-Mascaraque, L. G., Brodtkorb, A., & Drusch, S. (2022). The type of gum arabic affects interactions with soluble pea protein in complex coacervation. *Carbohydrate Polymers*, 295, 119851. <https://doi.org/10.1016/j.carbpol.2022.119851>
- Daoub, R. M. A., Elmubarak, A. H., Misran, M., Hassan, E. A., & Osman, M. E. (2018). Characterization and functional properties of some natural Acacia gums. *Journal of the Saudi Society of Agricultural Sciences*, 17(3), 241–249. <https://doi.org/10.1016/j.jssas.2016.05.002>
- de Kruijff, C. G., & Tuinier, R. (2001). Polysaccharide protein interactions. *Food Hydrocolloids*, 15(4), 555–563. [https://doi.org/10.1016/S0268-005X\(01\)00076-5](https://doi.org/10.1016/S0268-005X(01)00076-5)
- Dong, X., Wu, P., Cong, H., & Chen, X. D. (2022). Mechanistic study on in vitro disintegration and proteolysis of whey protein isolate gels: Effect of the strength of sodium ions. *Food Hydrocolloids*, 132, Article 107862. <https://doi.org/10.1016/j.foodhyd.2022.107862>
- Eratte, D., Wang, B., Dowling, K., Barrow, C. J., & Adhikari, B. P. (2014). Complex coacervation with whey protein isolate and gum arabic for the microencapsulation of omega-3 rich tuna oil. *Food & Function*, 5(11), 2743–2750. <https://doi.org/10.1039/c4fo00296b>
- Gu, Z., Liu, S., Duan, Z., Kang, R., Zhao, M., Xia, G., & Shen, X. (2021). Effect of citric acid on physicochemical properties and protein structure of low-salt restructured tilapia (*Oreochromis mossambicus*) meat products. *Journal of the Science of Food and Agriculture*, 101(4), 1636–1645. <https://doi.org/10.1002/jsfa.10784>
- Gulao, E. d. S., de Souza, C. J. F., Andrade, C. T., & Garcia-Rojas, E. E. (2016). Complex coacervates obtained from peptide leucine and gum arabic: Formation and characterization. *Food Chemistry*, 194, 680–686. <https://doi.org/10.1016/j.foodchem.2015.08.062>
- Harton, K., & Shimizu, S. (2019). Statistical thermodynamics of casein aggregation: Effects of salts and water. *Biophysical Chemistry*, 247, 34–42. <https://doi.org/10.1016/j.bpc.2019.02.004>
- Hei, Z. L., Zhao, M. H., Tian, Y. Y., Chang, H., Shen, X. R., Xia, G. H., & Wang, J. F. (2020). Isolation and characterization of a novel sialoglycopeptide promoting osteogenesis from *Gadus morhua* eggs. *Molecules*, 25(1), 156. <https://doi.org/10.3390/molecules25010156>
- Huang, Z. X., Lin, W. F., Zhang, Y., & Tang, C. H. (2022). Freeze-thaw-stable high internal phase emulsions stabilized by soy protein isolate and chitosan complexes at pH 3.0 as promising mayonnaise replacers. *Food Research International*, 156. <https://doi.org/10.1016/j.foodres.2022.111309>
- Jones, O. G., Lesmes, U., Dubin, P., & McClements, D. J. (2010). Effect of polysaccharide charge on formation and properties of biopolymer nanoparticles created by heat treatment of β -lactoglobulin-pectin complexes. *Food Hydrocolloids*, 24(4), 374–383. <https://doi.org/10.1016/j.foodhyd.2009.11.003>
- Kelley, J. J., & Tsai, A. C. (1978). Effect of pectin, gum arabic and agar on cholesterol absorption, synthesis, and turnover in rats. *The Journal of Nutrition*, 108(4), 630–639. <https://doi.org/10.1093/jn/108.4.630>
- Li, X., Hua, Y., Chen, Y., Kong, X., & Zhang, C. (2016). Protein selectivity controlled by polymer charge density and protein yield: carboxylated polysaccharides versus sulfated polysaccharides. *Journal of Agricultural and Food Chemistry*, 64(47), 9054–9062. <https://doi.org/10.1021/acs.jafc.6b03560>
- Lin, T. M., Kim, K. S., Karvinen, E., & Ivy, A. C. (1957). Effect of dietary pectin, protopectin and gum arabic on cholesterol excretion in rats. *The American Journal of Physiology*, 188(1), 66–70. <https://doi.org/10.1152/ajplegacy.1956.188.1.66>
- Liu, J., Shim, Y. Y., Wang, Y., & Reaney, M. J. T. (2015). Intermolecular interaction and complex coacervation between bovine serum albumin and gum from whole flaxseed (*Linum usitatissimum* L.). *Food Hydrocolloids*, 49, 95–103. <https://doi.org/10.1016/j.foodhyd.2015.02.035>
- Liu, S., Low, N. H., & Nickerson, M. T. (2009). Effect of pH, salt, and biopolymer ratio on the formation of pea protein isolate-gum arabic complexes. *Journal of Agricultural and Food Chemistry*, 57(4), 1521–1526. <https://doi.org/10.1021/jf802643n>
- Liu, Y., Liang, Q., Liu, X., Raza, H., Ma, H., & Ren, X. (2022). Treatment with ultrasound improves the encapsulation efficiency of resveratrol in zein-gum Arabic complex coacervates. *LWT – Food Science and Technology*, 153, Article 112331. <https://doi.org/10.1016/j.lwt.2021.112331>
- Liu, Z., Liu, C., Sun, X., Zhang, S., Yuan, Y., Wang, D., & Xu, Y. (2020). Fabrication and characterization of cold-gelation whey protein-chitosan complex hydrogels for the controlled release of curcumin. *Food Hydrocolloids*, 103, Article 105619. <https://doi.org/10.1016/j.foodhyd.2019.105619>
- Luo, W., Huang, H., Zhang, Y., Wang, F., Yu, J., Liu, Y., & Li, X. (2021). Complex coacervation behavior and the mechanism between rice glutelin and gum arabic at pH 3.0 studied by turbidity, light scattering, fluorescence spectra and molecular docking. *LWT – Food Science and Technology*, 150. <https://doi.org/10.1016/j.lwt.2021.112084>
- Meng, K., Chen, L., Xia, G., & Shen, X. (2021). Effects of zinc sulfate and zinc lactate on the properties of tilapia (*Oreochromis niloticus*) skin collagen peptide chelate zinc. *Food Chemistry*, 347, Article 129043. <https://doi.org/10.1016/j.foodchem.2021.129043>
- Morr, C. V., & Ha, E. Y. (1993). Whey protein concentrates and isolates: Processing and functional properties. *Critical Reviews in Food Science and Nutrition*, 33(6), 431–476. <https://doi.org/10.1080/10408399309527643>
- Muhoza, B., Qi, B., Harindintwali, J. D., Koko, M. Y. F., Zhang, S., & Li, Y. (2022). Combined plant protein modification and complex coacervation as a sustainable strategy to produce coacervates encapsulating bioactives. *Food Hydrocolloids*, 124. <https://doi.org/10.1016/j.foodhyd.2021.107239>
- Niu, F., Dong, Y., Shen, F., Wang, J., Liu, Y., Su, Y., & Yang, Y. (2015). Phase separation behavior and structural analysis of ovalbumin-gum arabic complex coacervation. *Food Hydrocolloids*, 43, 1–7. <https://doi.org/10.1016/j.foodhyd.2014.02.009>
- Ou, Z., & Muthukumar, M. (2006). Entropy and enthalpy of polyelectrolyte complexation: Langevin dynamics simulations. *The Journal of Chemical Physics*, 124(15), Article 154902. <https://doi.org/10.1063/1.2178803>
- Patel, S., & Goyal, A. (2015). Applications of natural polymer gum Arabic: A review. *International Journal of Food Properties*, 18(5), 986–998. <https://doi.org/10.1080/10942912.2013.809541>
- Pillai, P. K. S., Stone, A. K., Guo, Q., Guo, Q., Wang, Q., & Nickerson, M. T. (2019). Effect of alkaline de-esterified pectin on the complex coacervation with pea protein isolate

- under different mixing conditions. *Food Chemistry*, 284, 227–235. <https://doi.org/10.1016/j.foodchem.2019.01.122>
- Plati, F., & Paraskevopoulou, A. (2023). Hemp protein isolate–gum Arabic complex coacervates as a means for oregano essential oil encapsulation. Comparison with whey protein isolate–gum Arabic system. *Food Hydrocolloids*, 136, Article 108284. <https://doi.org/10.1016/j.foodhyd.2022.108284>
- Rocha, C. M., Souza, H. K., Magalhães, N. F., Andrade, C. T., & Gonçalves, M. P. (2014). Rheological and structural characterization of agar/whey proteins insoluble complexes. *Carbohydrate Polymers*, 110, 345–353. <https://doi.org/10.1016/j.carbpol.2014.04.015>
- Santos, M. J., Teixeira, J. A., & Rodrigues, L. R. (2012). Fractionation of the major whey proteins and isolation of β -Lactoglobulin variants by anion exchange chromatography. *Separation and Purification Technology*, 90, 133–139. <https://doi.org/10.1016/j.seppur.2012.02.030>
- Sharifi, S., Rezaad-Bari, M., Alizadeh, M., Almasi, H., & Amiri, S. (2021). Use of whey protein isolate and gum Arabic for the co-encapsulation of probiotic *Lactobacillus plantarum* and phytosterols by complex coacervation: Enhanced viability of probiotic in Iranian white cheese. *Food Hydrocolloids*, 113. <https://doi.org/10.1016/j.foodhyd.2020.106496>
- Shimizu, S. (2011). The effect of urea on hydrophobic hydration: Preferential interaction and the enthalpy of transfer. *Chemical Physics Letters*, 517(1–3), 76–79. <https://doi.org/10.1016/j.cplett.2011.10.011>
- Smithers, G. W., John Ballard, F., Copeland, A. D., de Silva, K. J., Dionysius, D. A., Francis, G. L., & Regester, G. O. (1996). New opportunities from the isolation and utilization of whey proteins. *Journal of Dairy Science*, 79(8), 1454–1459. [https://doi.org/10.3168/jds.S0022-0302\(96\)76504-9](https://doi.org/10.3168/jds.S0022-0302(96)76504-9)
- Tavares, L., Souza, H. K. S., Gonçalves, M. P., & Rocha, C. M. R. (2021). Physicochemical and microstructural properties of composite edible film obtained by complex coacervation between chitosan and whey protein isolate. *Food Hydrocolloids*, 113, Article 106471. <https://doi.org/10.1016/j.foodhyd.2020.106471>
- Tavares, L., & Zapata Norena, C. P. (2019). Encapsulation of garlic extract using complex coacervation with whey protein isolate and chitosan as wall materials followed by spray drying. *Food Hydrocolloids*, 89, 360–369. <https://doi.org/10.1016/j.foodhyd.2018.10.052>
- Turgeon, S. L., Schmitt, C., & Sanchez, C. (2007). Protein–polysaccharide complexes and coacervates. *Current Opinion in Colloid & Interface Science*, 12(4), 166–178. <https://doi.org/10.1016/j.cocis.2007.07.007>
- Wang, L., Zhang, H., Li, H., Zhang, H., Chi, Y., Xia, N., & Rayan, A. M. (2022). Fabrication and digestive characteristics of high internal phase Pickering emulsions stabilized by ovalbumin-pectin complexes for improving the stability and bioaccessibility of curcumin. *Food Chemistry*, 389. <https://doi.org/10.1016/j.foodchem.2022.133055>
- Weinbreck, F., de Vries, R., Schrooyen, P., & de Kruif, C. G. (2003). Complex coacervation of whey proteins and gum arabic. *Biomacromolecules*, 4(2), 293–303. <https://doi.org/10.1021/bm025667n>
- Weinbreck, F., Minor, M., & De Kruif, C. G. (2004). Microencapsulation of oils using whey protein/gum arabic coacervates. *Journal of Microencapsulation*, 21(6), 667–679. <https://doi.org/10.1080/02652040400008499>
- Xiong, W., Ren, C., Jin, W., Tian, J., Wang, Y., Shah, B. R., & Li, B. (2016). Ovalbumin-chitosan complex coacervation: Phase behavior, thermodynamic and rheological properties. *Food Hydrocolloids*, 61, 895–902. <https://doi.org/10.1016/j.foodhyd.2016.07.018>
- Yan, J. N., Nie, B., Jiang, X. Y., Han, J. R., Du, Y. N., & Wu, H. T. (2020). Complex coacervation of scallop (*Patinopecten yessoensis*) male gonad hydrolysates and κ -carrageenan: Effect of NaCl and KCl. *Food Research International*, 137, Article 109659. <https://doi.org/10.1016/j.foodres.2020.109659>
- Yang, S., Li, X., Hua, Y., Chen, Y., Kong, X., & Zhang, C. (2020). Selective complex coacervation of pea whey proteins with chitosan to purify main 2S albumins. *Journal of Agricultural and Food Chemistry*, 68(6), 1698–1706. <https://doi.org/10.1021/acs.jafc.9b06311>
- Yao, X., Xiang, S., Nie, K., Gao, Z., Zhang, W., Fang, Y., & Jiang, F. (2016). Whey protein isolate/gum arabic intramolecular soluble complexes improving the physical and oxidative stabilities of conjugated linoleic acid emulsions. *RSC Advances*, 6(18), 14635–14642. <https://doi.org/10.1039/c5ra26040j>
- Yao, X., Xu, K., Shu, M., Liu, N., Li, N., Chen, X., & Jiang, F. (2021). Fabrication of iron loaded whey protein isolate/gum Arabic nanoparticles and its adsorption activity on oil-water interface. *Food Hydrocolloids*, 115. <https://doi.org/10.1016/j.foodhyd.2021.106610>
- Zhang, J., Jia, G., Wanbin, Z., Minghao, J., Wei, Y., Hao, J., & Sun, A. (2021). Nanoencapsulation of zeaxanthin extracted from *Lycium barbarum* L. by complex coacervation with gelatin and CMC. *Food Hydrocolloids*, 112. <https://doi.org/10.1016/j.foodhyd.2020.106280>
- Zhang, Q., Dong, H. M., Gao, J., Chen, L. Y., & Vasanthan, T. (2020). Field pea protein isolate/chitosan complex coacervates: Formation and characterization. *Carbohydrate Polymers*, 250. <https://doi.org/10.1016/j.carbpol.2020.116925>
- Zhou, B., Tobin, J. T., Drusch, S., & Hogan, S. A. (2021). Dynamic adsorption and interfacial rheology of whey protein isolate at oil-water interfaces: Effects of protein concentration, pH and heat treatment. *Food Hydrocolloids*, 116, Article 106640. <https://doi.org/10.1016/j.foodhyd.2021.106640>
- Zhou, S., Han, L., Lu, K., Qi, B., Du, X., Liu, G., & Li, Y. (2022). Whey protein isolate-phytosterols nanoparticles: Preparation, characterization, and stabilized food-grade pickering emulsions. *Food Chemistry*, 384. <https://doi.org/10.1016/j.foodchem.2022.132486>
- Zou, W., Mourad, F. K., Zhang, X., Ahn, D. U., Cai, Z., & Jin, Y. (2020). Phase separation behavior and characterization of ovalbumin and propylene glycol alginate complex coacervates. *Food Hydrocolloids*, 108. <https://doi.org/10.1016/j.foodhyd.2020.105978>